DESIGN OF AN IMPROVED S-BAND SLED PULSE COMPRESSOR

Pengbin Huang, Yelong Wei†, Yihao Zhang, Zexin Cao, Zhicheng Huang, Guangyao Feng,
University of Science and Technology of China, Hefei, China

Abstract

This paper presents the design of an improved SLED pulse compressor for our beam test platform at National Synchrotron Radiation Laboratory (NSRL). It consists of a 3 dB hybrid, a TE_{10}-TE_{01} mode converter, and a resonator storage cavity. Through geometrical optimizations, the resonator is designed to operate in the $TE_{0,1,10}$ mode, which offers a high intrinsic quality factor while maintaining cost-effectiveness. Additionally, the conventional cylindrical configuration has been modified to a double-ended conical structure, which facilitates better mode isolation.

INTRODUCTION

RF pulse compression is widely used to increase peak RF power when the klystron pulse length is long compared with the pulse required by an accelerating structure. In a SLED-I system two identical storage cavities are filled through a 3 dB hybrid coupler and, near the end of the drive pulse, the incident phase is reversed by 180 degrees to release the stored energy into a shorter, higher power pulse [1]. Compact high-power systems require high intrinsic quality factor and stable mode operation. TE01-like cylindrical modes are attractive because the magnetic field in the wall is small, enabling high Q_o, while adiabatic tapers transitions can suppress excitation of unwanted modes and reduce the size of the mode converters [2],[3].

DESIGN REQUIREMENTS

The compressor comprises (i) a four-port 3 dB hybrid for power splitting/combining and source isolation, (ii) two identical $TE_{0,1,10}$ storage cavities, and (iii) a compact TE_{10}-TE_{01} mode converter to connect a rectangular waveguide input to the circular cavity. Fig. 1 demonstrates the prototype pulse compressor of the CERN BOX2 SLED. Figure 2 shows a block diagram of the proposed configuration. The intended operating point is 2.9982 GHz with 4 us input pulses at 50 Hz repetition. Low-power acceptance is specified by input intrinsic quality factor, while pulse-compression performance is expressed by peak and average power gains at the required compressed pulse length.

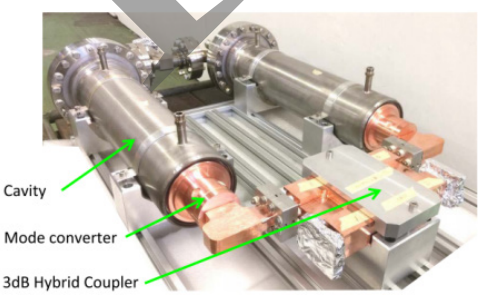

Figure 1: CERN BOX2 SLED.

†wylong@ustc.edu.cn

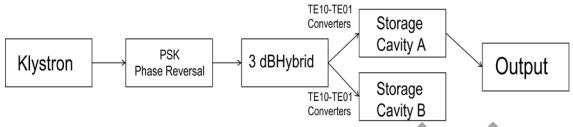

Figure 2: Block diagram of the improved SLED-I pulse compressor with two storage cavities and a 3 dB hybrid [4].

Table 1: Main Design Targets of the S-band Pulse Compressor

Parameter	Target	Unit
Operating frequency	2.9982	GHz
Repetition	50	Hz
Input pulse width /	4	us
Output pulse width	0.8	μs
Input power	45	MW
Cavity mode	$TE_{0,1,10}$	-
Q_o	>=95,000	-
Peak	>= 5	-
Average power gain	>= 3	-

$TE_{0,1,10}$ STORAGE CAVITY WITH PARAMETRIC ADIABATIC TAPERS

The time - domain method [1] directly characterizes the pulse compression process through the analysis of the transient behavior of resonant cavities. This approach can be integrated with frequency - domain analysis for verification. By utilizing rectangular pulses as ideal input pulses, any pulse compressor can be assessed based on the following key parameters:

$$M = \frac{1}{t_2 - t_1} \frac{\int_{t_1}^{t_2} P_{out}(t)\,\mathrm{d}t}{\int_{t_1}^{t_2} P_{in}(t)\,\mathrm{d}t} = \frac{\int_{t_1}^{t_2} P_{out}(t)\,\mathrm{d}t}{\int_{t_1}^{t_2} P_{in}(t)\,\mathrm{d}t} \quad . \qquad (1)$$

Where t_1 denotes the phase inversion time, t_2 represents the input pulse width, M indicates the equivalent power amplification factor within the duration of a radio frequency pulse. The parameter analysis of the mode converter is shown in Fig. 3.

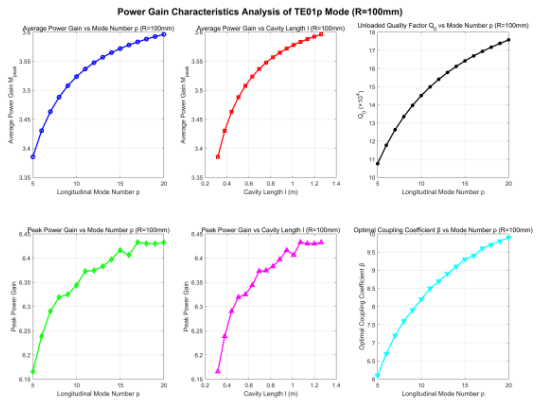

Figure 3: Analysis of cavity mode and related parameters.

The structure of the resonant cavity is shown in Fig. 4. For SLED-I systems containing adiabatic cones, the analysis of corresponding power gain coupling can be conducted using cylindrical models, while Q-value and frequency analysis requires the equivalent method. This study approximates complex continuous gradient segments as equivalent cylinders with radius $R_{avg} = (R1 + R2)/2$ (where R1 is the main cavity radius and R2 is the end radius). By combining the local resonant frequency f_1 of the main cavity with the local frequency f_2 of the equivalent gradient segment, the overall hybrid equivalent frequency can be derived through physical length weighting.

$$f_{mix} = \frac{H_1 \cdot f_1 + 2H_2 \cdot f_2}{H_1 + 2H_2} \quad . \tag{2}$$

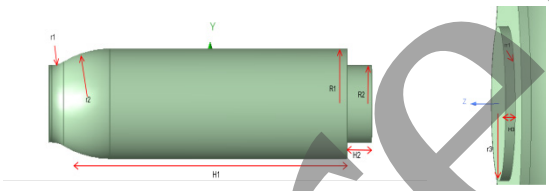

Figure 4: Structure of $TE_{0,1,10}$ resonator. (a) cavity body (b) coupling iris.

Table 2: Basic Parameter Table of Resonator

Parameter	Value	Unit
R1	100	mm
H1	558.24	mm
R2	70.13	mm
H2	50.65	mm
r1	50	mm
r2	200	mm
r3	39.68	mm
H3	13.3	mm
rr1	3.54	mm

The resonant cavity is composed of parameters listed in Table 2. These parameters can be tuned to meet the frequency target, manage mode spacing, and improve matching to the mode converter. Geometric optimization is included at joints and around the coupling iris to reduce peak magnetic field and to mitigate pulse heating. And the simulation results are shown in Fig. 5 and Fig. 6.

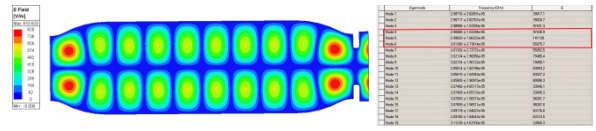

Figure 5: (a) Simulated electric field of the TE0,1,10 mode in the improved storage cavity with adiabatic tapers. (b) Q0 and mode frequency interval.

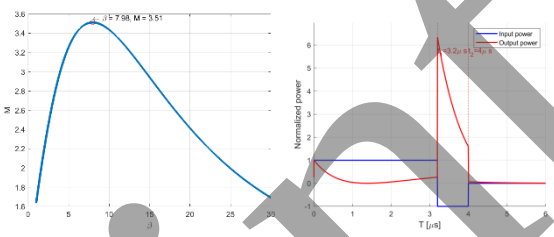

Figure 6: The relationship between the average power gain M of the pulse compressor output characteristics and the coupling coefficient β. (b) input-output result of the cavity operating in $TE_{0,1,10}$ mode.

TE_{10}-TE_{01} MODE CONVERTER AND 3DB HYBRID

The RF network must deliver high power with low reflection and provide isolation of the klystron during the cavity discharge. Two key components are the TE10-TE01 mode converter and the 3 dB hybrid.

Four-port 3 dB Hybrid

A four-port, 3-dB hybrid provides equal power splitting to the two storage cavities, which have a quadrature phase relationship which is shown in Fig. 7. It also recombines the emitted waves during phase reversal, ensuring that the source port remains isolated while power is delivered to the load port. The design was optimized for amplitude balance and phase accuracy around 2.9982 GHz.

The 3dB Hybrid S-parameter is below -45dB at the target frequency.

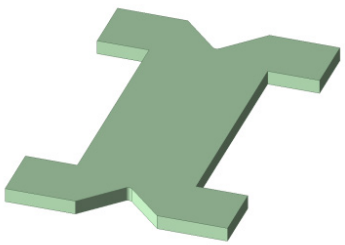

Figure 7: Structure of the 3dB Hybrid.

Compact TE_{10}-TE_{01} Mode Converter

A compact mode converter transforms the rectangular waveguide TE_{10} mode to a TE_{01} mode suitable for feeding the cylindrical cavity (Fig. 8). A short multistep approach is used: TE_{10} is first transformed into an intermediate mode

in a compact rectangular section and then launched into a circular where matching posts are used to minimize reflection and suppress competing modes. The compact converter reduces sensitivity to assembly length and enables integration within the required space.

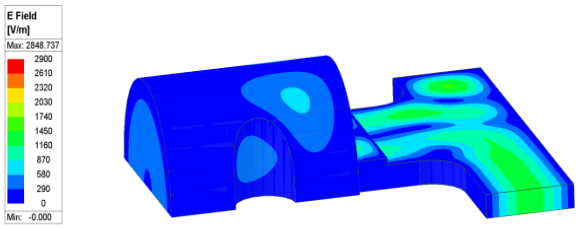

Figure 8: Simulation diagram of the mode converter.

The mode converter achieves excellent performance with a reflection below -50dB.

SIMULATIONS AND DISCUSSIONS

The overall assembly results are shown in Figure 8, with mutual validation conducted using HFSS and CST. Since CST better simulates copper wrapped on vacuum layer surfaces, the CST model on the right is depicted in yellow. The coupling degree and reflection results are illustrated in Fig. 9.

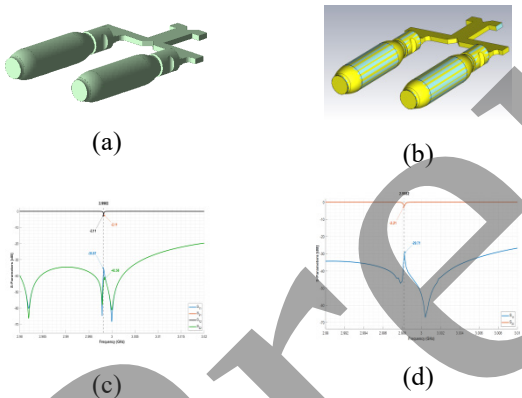

(a) (b)

(c) (d)

Figure 9: (a) Full assembly diagram of pulse compressor in HFSS. (b) Full assembly diagram of pulse compressor in CST. (c) simulation results of pulse compressor HFSS (d) simulation results of pulse compressor CST.

Analysis of Fig. 9 (c) and Fig. 9 (d) reveals that the coupling degrees of 7.70 and 7.90 respectively yield essentially consistent results, with reflection levels below-30dB.

Eigenmode simulations in HFSS [5] and CST [6] were used to tune the $TE_{0,1,10}$ frequency to 2.9982 GHz while maintaining a minimum mode separation of about 10 MHz in the neighbourhood of the operating mode. With oxygen-free copper walls, the intrinsic Q is predicted to be near 140000, exceeding the acceptance threshold of 95,000. After assembling the mode converter and hybrid, the coupling iris was adjusted to reach a coupling factor beta around 8, corresponding to an on-resonance reflection magnitude of about -2.2 dB. Time-domain calculations using standard SLED relations indicate peak power gain above 6 and average gain above 3.5 for 4 us input and 0.8 us compressed output.

And our magnetic field results are less than 0.22 MA/m, with pulse temperature rise below 22 ℃.

CONCLUSION

An improved S-band SLED-I pulse compressor has been designed with $TE_{0,1,10}$ storage cavities employing parametric adiabatic tapers. The key geometric variables (R1, H1, R2, H2) provide tuning flexibility and support stable single-mode operation while simplifying the TE10-TE01 conversion. Simulations indicate that the design can satisfy low-power acceptance criteria and achieve peak compression gains consistent with the high-power requirements. Future work will include fabrication, low-power RF measurements, and high-power testing with temperature and vacuum conditioning.

ACKNOWLEDGMENT

This work is supported by the "Hundred Talents Program" of Chinese Academy of Sciences (Grant No. KJ2310007003); the Fundamental Research Funds for the Central Universities (Grant No. WK2310000114); the Chinese Academy of Sciences President's International Fellowship Initiative (Grant No. 2025PD0102); the 12th Research Institute of China Electronics Technology Group Corporation (Grant No. K2301287).

REFERENCES

[1] Z. D. Farkas, H. A. Hogg, G. A. Loew, and P. B. Wilson, "Recent Progress on Sled, The SLAC Energy Doubler," *IEEE Trans. Nucl. Sci.*, vol. 22, no. 3, pp. 1299–1302, 1975. doi:10.1109/tns.1975.4327871

[2] B. Woolley, I. Syratchev, and A. Dexter, "Control and performance improvements of a pulse compressor in use for testing accelerating structures at high power," *Phys. Rev. Accel. Beams*, vol. 20, no. 10, Oct. 2017. doi:10.1103/physrevaccelbeams.20.101001

[3] D. Gudkov, S. Lebet, R. Leuxe, A. Olyunin, G. Riddone, *et al.*, "General purpose X-band High RF power components developed within CLIC collaboration" in *Proc. KEK*, Tsukuba, 2012.

[4] Shen Xuming, Zhang Peng, and He Tianhui, "High power microwave pulse compression of energy doublers," *High Power Laser Part. Beams,* vol. 22, no. 4, pp. 849 – 852, 2010. doi:10.3788/hplpb20102204.0849

[5] Ansys HFSS, Release 2023 R1, Ansys, Inc., Canonsburg, PA, USA, 2023, https://www.ansys.com.

[6] CST Studio Suite, version 2023, Dassault Systems, Vélizy-Villacoublay, France, 2023, https://www.3ds.com.